Prototyping Energy Harvesting Active Networked Tags (EnHANTs)

Maria Gorlatova*, Robert Margolies*, John Sarik*, Gerald Stanje*, Jianxun Zhu*, Baradwaj Vigraham*,
Marcin Szczodrak†, Luca Carloni†, Peter Kinget*, Ioannis Kymissis*, Gil Zussman*
*Electrical Engineering, †Computer Science, Columbia University, New York, NY, 10027
{mag2206, rsm2156, jcs2160, gs2604, jz2382, bv2152, mks2158}@columbia.edu
{luca@cs, kinget@ee, johnkym@ee, gil@ee}.columbia.edu

***Abstract*—This paper focuses on a new type of wireless devices in the domain between RFIDs and sensor networks – Energy Harvesting Active Networked Tags (EnHANTs). Future EnHANTs will be small, *flexible*, and *self-powered* devices that can be attached to objects that are traditionally not networked (e.g., books, toys, clothing), thereby providing the infrastructure for novel tracking applications. We present the design considerations for the EnHANT prototypes, developed over the past 3 years. The prototypes harvest indoor light energy using custom *organic solar cells*, communicate and form *multihop networks* using ultra-low-power *Ultra-Wideband Impulse Radio (UWB-IR) transceivers*, and adapt their communications and networking patterns to the energy harvesting and battery states. We also describe a small scale EnHANTs testbed that uniquely allows evaluating different algorithms with trace-based light energy inputs.**

***Index Terms*—Energy adaptive networking, energy harvesting, ultra-low-power communications, organic solar cells, ultra-wideband (UWB), cross-layer.**

I. Introduction

This paper focuses on the design and prototyping of a new type of ultra-low-power device - Energy Harvesting Active Networked Tag (EnHANT). EnHANTs will be *self-powered*, flexible, and small wireless tags that harvest indoor light energy and can be attached to objects that are traditionally not networked. The realization of the EnHANTs vision is based on recent advances in *energy harvesting* [5], [12] and on the ability to fabricate Organic Photovoltaics[1] (OPVs) on *flexible substrates* [9], which will enable the pervasive use of future flexible tags (a custom-designed flexible OPV is shown in Fig. 1(a)). Another enabling technology is ultra-low-power Ultra-Wideband Impulse-Radio (UWB-IR) communications [3], [10]. Due to its *pulse-based* nature, UWB-IR spends substantially less energy than other low-power wireless technologies [5]. A form factor for the envisioned EnHANT is shown in Fig. 1(b). Harvesting indoor light energy[2], a tag of this size (less than 3.5x3.5cm) will support continuous data rates between 1 and 13kpbs [7].

EnHANTs will be one of the enablers for the *Internet of Things* [5], and will support a variety of tracking and monitoring applications beyond what current tracking technology, RFIDs, permits. In [5] we described a representative EnHANT application: *locating a misplaced book in a library*. In this application, EnHANTs will be attached to library books, harvest indoor light energy, and wirelessly exchange IDs with the neighboring books. If a book is misplaced, its ID will be significantly different from the IDs of its neighbors, and this information will be forwarded to the librarian. Additional representative EnHANTs applications include finding items with particular characteristics in a store or a warehouse, and continuous peer monitoring of goods in transit.

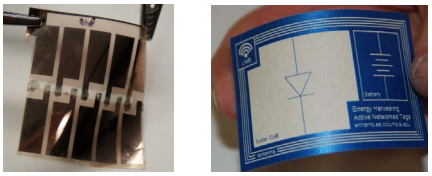

(a) (b)

Fig. 1. (a) A custom-designed flexible organic solar cell (photovoltaic), and (b) the intended EnHANT form factor.

Combining the advances in energy harvesting and ultra low power communications has attracted considerable attention (e.g., [1], [12]). Moreover, networking protocols for energy harvesting nodes have been recently proposed (e.g., [2], [4], [7], [8]). However, the challenges imposed by the cross layer interactions between energy harvesting, RF transceiver design, communications, and networking have not been studied in depth [5]. Hence, we present the design considerations of the EnHANT prototypes (shown in Fig. 2) and testbed (shown in Fig. 3), developed over the past 3 years in 5 integration phases, each demonstrated in a conference (e.g., [11]).[3]

The prototypes form small networks and adapt their communications and networking patterns to the battery and energy harvesting states. To the best of our knowledge, they are *the first wireless devices that harvest energy using OPVs*, *the first to demonstrate multihop data forwarding over the ultra low power UWB-IR physical layer*, and *the first to adapt to the harvesting states in real time*. Additionally, while a few energy harvesting testbeds exist (e.g., [12]), to the best of our

[1]We use the term *photovoltaic* rather than *solar cell* to emphasize the use for harvesting *indoor light*, rather than sunlight.

[2]Indoors, the amount of energy available is a *thousand times lower* than outdoors [5].

[3]A video showing the testbed is available at youtu.be/QFCf62lBATI .

978-1-4673-5946-7/13/$31.00 ©2013 IEEE

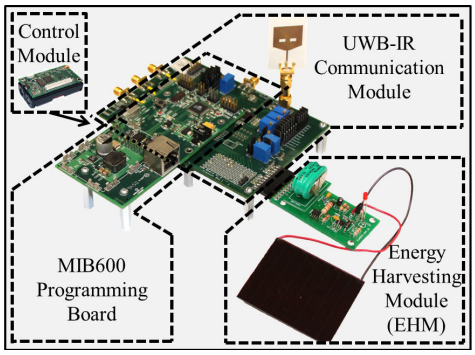

Fig. 2. An EnHANT prototype.

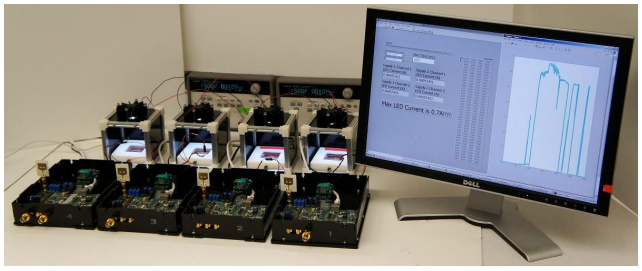

Fig. 3. A software-based light control system, along with 4 EnHANT prototypes.

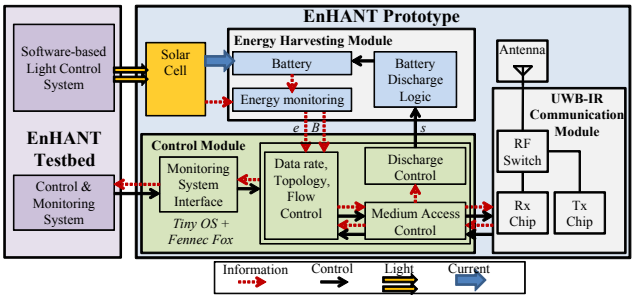

Fig. 4. A block diagram of the EnHANT prototype, and its interactions with the testbed.

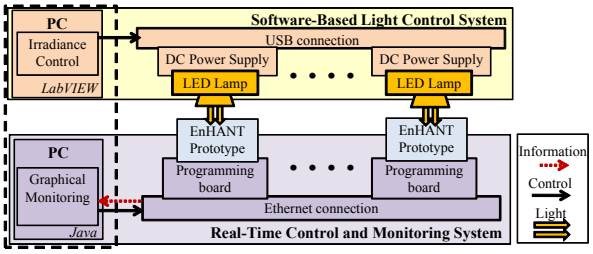

Fig. 5. A schematic diagram of the EnHANTs testbed.

knowledge, the EnHANTs testbed is the first to support trace-based *light energy control* functionality.

The paper is organized as follows. Section II discusses the related work. Section III presents an overview of the prototypes and the testbed. Section IV discusses the OPVs, Energy Harvesting Module, and energy allocation policies for energy harvesting nodes. Section V discusses the UWB-IR transceiver, Medium Access Control (MAC) layer, and higher-layer protocols. We conclude the paper in Section VI. Due to space constraints, many details are omitted and appear in a technical report [6].

II. Related Work

As mentioned above, numerous algorithms for energy harvesting nodes have been developed [2], [4], [7], [8]. Yet, implementations and performance evaluations with energy harvesting hardware are rare [12], [14]. Unlike the EnHANT prototypes, similar systems (e.g., [13]) do not provide real time harvesting rate information and offer only limited energy awareness. Existing sensor network nodes that harvest energy from sunlight [12] and indoor light [1] typically use monocrystalline or amorphous silicon (a-Si) solar cells, rather than OPVs which are used in EnHANTs.

The prototypes support MAC and networking functionalities over the UWB-IR physical layer. Other UWB-IR implementations (e.g., [10] and references therein) do not include a network of more than two nodes. Additionally, although MAC protocols for UWB-IR exist (e.g., [15] and references therein), no evaluations or higher layer communications have been reported. Our MAC layer overcomes difficulties in implementing Carrier Sense Multiple Access (CSMA) over UWB-IR [15].

III. Prototype and Testbed

Prototype: The EnHANT prototype is shown in Fig. 2 and its block diagram, including the different modules and their interactions, is shown in Fig. 4. The current prototypes are larger than the envisioned node that appears in Fig. 1(b)[4], yet they are already integrated with the enabling technologies.

The prototype's Energy Harvesting Module (EHM) contains a rechargeable battery and energy monitoring circuitry. It interfaces with the solar cell, which is designed to harvest *indoor light energy*. The prototypes communicate with each other wirelessly using ultra-low-power UWB-IR Communication Modules, based on UWB-IR transmitter and receiver chips (described in [3]).[5] The custom chips are mounted onto a printed circuit board that interfaces with the other prototype components. A Complex Programmable Logic Device is used as the glue logic between the radio chipset and the rest of the prototype.

The Control Module (CM) is based on a legacy MICA2 mote that runs TinyOS with an added Fennec Fox software framework. The CM implements the MAC and higher layers of the networking stack. The Communication Module is integrated with the CM such that packets originating in the TinyOS application layer are sent *wirelessly via the UWB-IR transceiver*. The CM adapts the prototype's networking and communication patterns, based on the energy states reported by the EHM.

Testbed: Our small scale testbed, shown schematically in Fig. 5, includes *6 EnHANT* prototypes, a *control and monitoring* system, and a *software-based light control system*. For control and monitoring, the prototypes are placed on MIB600

[4]A discussion on achieving the intended node form factor appears in [6].

[5]While the transceiver chips were described in [3], the overall UWB-IR Communication Module was developed specifically for this paper.

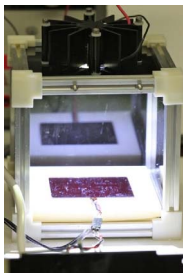

Fig. 6. A dark box enclosure used in the light control system.

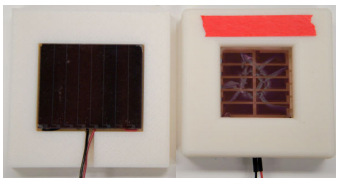

(a) (b)

Fig. 7. Solar cells integrated with EnHANT prototypes: (a) an amorphous silicon (a-Si) solar cell, and (b) a custom-fabricated Organic Photovoltaic (OPV).

programming boards and accessed from a PC via Ethernet. On the PC, a Java-based graphical monitoring system shows in real time the network topology, data rates, energy harvested, battery levels, and the individual packets transmitted.

The software-based light control system allows exposing individual prototypes to repeatable light energy conditions *based on real-world irradiance (light energy) traces*. The system is shown in Fig. 3, and the hardware design considerations appear in [6]. To ensure full control over light conditions, the photovoltaics are placed inside custom-designed dark box enclosures, shown in Fig. 6. A LabVIEW script on a PC controls the irradiance inside each enclosure. This system allows replicating traces with remarkable repeatability. For example, energy harvesting rate variations over 8 repetitions of a light energy trace are shown using errorbars in Fig. 10(a).[6] This ensures that experimental evaluations of energy harvesting adaptive policies are *based on the same energy inputs*.

IV. Energy Harvesting

In this section we briefly describe the photovoltaics and the EHM. We also evaluate a few energy allocation policies for energy harvesting nodes, using the light energy traces from [7].

A. Photovoltaics and the Energy Harvesting Module (EHM)

We equipped the EnHANT prototypes with custom-designed *OPVs* (that can be made *flexible*) and with commercially available rigid amorphous silicon (a-Si) solar cells that are commonly used for indoor harvesting applications [1]. The photovoltaics are shown in Fig. 7. The two types of solar cells can be easily interchanged, as can be seen in Fig. 2.

Different types of photovoltaics perform differently under the same light conditions. For example, the harvesting efficiency of the OPVs is 1%, while for a-Si cells it varies between 1% and 3% depending on the irradiance (see the measurement results in Fig. 8(a)). Correspondingly, as shown in Fig. 8(c), when we expose the two photovoltaics to irradiance levels based on a light energy trace recorded over a day in L-1 [7] (Fig. 8(b)), *the curves of the power generated by the two photovoltaics have different shapes*. We note that these effects are difficult to capture in simulations (e.g., [4], [7]), which simply assume that the energy harvested by a solar cell is a linear function of the irradiance.

The EHM stores the energy harvested by a photovoltaic in a rechargeable battery. A block diagram and a photo of the EHM are shown in Fig. 9, and the hardware design considerations are provided in [6]. The EHM interactions with the other prototype components are shown in Fig. 4. The EHM monitors, in near real time, the battery level, $B(i)$, and the energy harvesting rate, $e(i)$, and reports them to the CM. *The EHM does not supply energy to the other EnHANT prototype components*. Rather, as shown in Fig. 4, the EHM implements *controlled energy spending functionality*, where, in correspondence with transceiver energy spending on transmitting and receiving packets, the CM signals to the EHM to activate a small load, which spends energy at a requested rate $s(i)$. Releasing the constraint of running the prototype using harvested energy allows us to experiment with various hardware and protocol configurations.

B. Node Energy Allocation Policies

Different *energy allocation policies* for energy harvesting nodes have been proposed [4], [7]. We evaluate a set of simple policies that aim to achieve *energy neutrality* – full, yet not excessive, spending of the energy harvested. These policies, briefly described below, closely match node energy spending rates, $s(i)$, to node energy harvesting rates, $e(i)$.

Exponential Policies (EX): The desired energy spending rate $s'(i)$ is set to the *exponential average* of the energy harvesting rate: $s'(i) \leftarrow \widehat{e}(i) = \alpha \cdot \widehat{e}(i-1) + (1-\alpha) \cdot e(i)$, $0 \leq \alpha \leq 1$. Similar policies were evaluated, via simulations, in [8].

Energy Profile-based Policies (EP-K): A node creates an *energy profile* $\{\overline{e}(1), ..., \overline{e}(K)\}$ by determining its *expected harvesting rate*, $\overline{e}(i)$, for different time intervals i. Energy profiles are used as inputs to many proposed policies [4], [7], [8]. In the EP-K policies (K corresponds to the number of time intervals), the node's desired energy spending rates are set to the expected energy harvesting rates: $s'(i) \leftarrow \overline{e}(i)\ \forall i \in K$. For example, the EP-1 policy (examined, via simulations, in [4], [7]), corresponds to a node spending energy at its *average expected harvesting rate* over the entire planning horizon.

We conducted extensive experiments with different EX and EP-K policies, providing nodes, equipped with either an a-Si solar cell or an OPV, a dynamic light energy input based on the light energy traces from [7]. Examples of energy spending rates, recorded in prototypes running these policies, are shown in Fig. 10(b). They are obtained for node energy harvesting rates illustrated in Fig. 10(a).

The experimental results and the results obtained via MATLAB simulations *closely match*. For example, for the policies shown in Fig. 10(c), the largest mismatch between the experimentally recorded and simulated battery levels was 5mC (one battery resolution level of the EHM). This confirms the reliability and precision of the energy state monitoring and controlled energy spending functionalities of the EHM.

[6]We provided the prototype with a light input corresponding to the light energy recorded over a day in location L-3 [7], compressed to 321s and scaled by 2.1x. The prototype was equipped with an a-Si solar cell. In the 8 experiments, the variability in total energy harvested was *under 1.9%*.

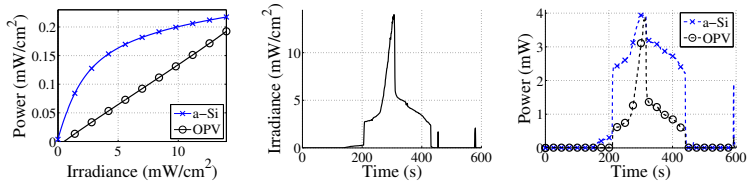

(a) (b) (c)

Fig. 8. Energy harvesting for a prototype with an a-Si solar cell and an Organic Photovoltaic (OPV): (a) generated power as a function of irradiance (light intensity), (b) time-varying irradiance based on a light energy trace from [7], (c) power harvested by an a-Si solar cell and an OPV.

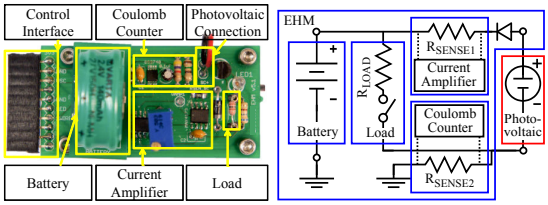

(a) (b)

Fig. 9. (a) A photo of the Energy Harvesting Module (EHM), and (b) its block diagram.

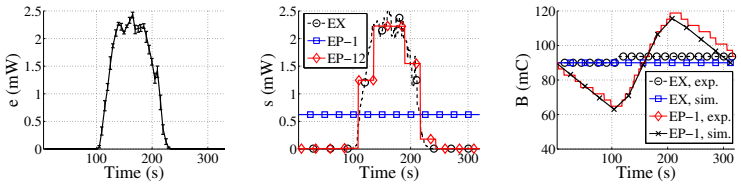

(a) (b) (c)

Fig. 10. Node energy allocation policies: (a) energy harvesting rates, (b) energy spending rates under the EX, EP-1, and EP-12 policies, and (c) battery levels, experimentally measured and simulated, under the EX and EP-1 policies.

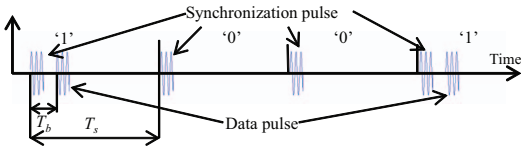

Fig. 11. S-OOK modulation and parameters.

The EX and EP-K policies effectively ensure energy neutrality. For example, in all our experiments with the EX and EP-K policies corresponding to node energy harvesting rates shown in Fig. 10(a), the node used *95%-96% of the energy harvested*. In future work, we will evaluate larger-scale energy harvesting adaptive policies (i.e., link and network) which use these policies as 'building blocks'.

V. UWB-IR Communications, Medium Access Control (MAC), and Higher-Layer Algorithms

The EnHANT prototypes communicate using ultra-low-power Ultra-Wideband Impulse Radio (UWB-IR) transceivers which are *fundamentally different* from narrow-band transceivers. In UWB-IR, information is transmitted using short *pulses* and most of the transceiver circuitry can be shut down between the pulses, resulting in significant power savings [5]. Yet, pulse-based communications pose many challenges including, for example, the implementation of Clear Channel Assessment (CCA) functionality. Additionally, in UWB-IR the energy required to receive a bit is an order of magnitude higher than the energy to transmit [3], [5].

A. UWB-IR Chipset and EnHANT Prototype Integration

The UWB-IR transceiver [3] operates in a 500MHz band around a center frequency of 3.8GHz. The modulation scheme is Synchronized On-Off Keying (S-OOK), shown in Fig. 11, which permits low power timing acquisition. An S-OOK symbol consists of a synchronization pulse, which is always present, and a data pulse, which is only present for a '1' bit. These pulses are separated by a time interval T_b. Adjacent symbols are separated by a time interval T_s. We currently use $T_b = 1\mu$s, $T_s = 54\mu$s, for a transmission rate of 18.5kbps.

The UWB-IR Communication Module, shown in Fig. 2 and schematically described in Fig. 4 (as part of the EnHANT prototype diagram), is implemented on a dedicated printed circuit board, and is interfaced with an omnidirectional UWB antenna. To integrate the UWB-IR transceiver with the protocol stack, we developed a device driver that provides an abstract interface to the MAC layer, and functionalities such as packet serialization, buffering, and CCA. *Previous work on MAC for UWB-IR assumes that performing CCA is impossible* due to the lack of a carrier waveform and interference from narrowband sources [15]. Yet, we managed to implement CCA using a simple threshold-based energy detector. The receiver chip listens for an output pulse for $2 \cdot T_b$; if no pulse is demodulated, the channel is declared idle. Energy spikes from interfering systems may cause CCA to falsely report a busy channel. However, for our purposes, these CCA 'false alarms' do little to affect our application which can wait until the noise spikes dissipate to transmit a packet.

We extensively characterized the UWB-IR communication module's sensitivity to narrowband interference, transmission rate limits, and packet error rates. Among other things, we have shown that it operates with a packet success rate over 95% at distances up to a meter. Additional module design considerations and experimental characterizations appear in [6].

B. Medium Access Control (MAC)

To verify the experimental UWB-IR physical layer and enable upper layer protocols, we implemented two basic MAC protocols: p-persistent CSMA (enabled by our implementation of CCA) and slotted Aloha.[7] While more sophisticated

[7] In slotted Aloha, given a packet, a node transmits in a slot with probability p. In p-persistent CSMA, with probability p, a node senses the channel. If the channel is determined to be idle, it transmits.

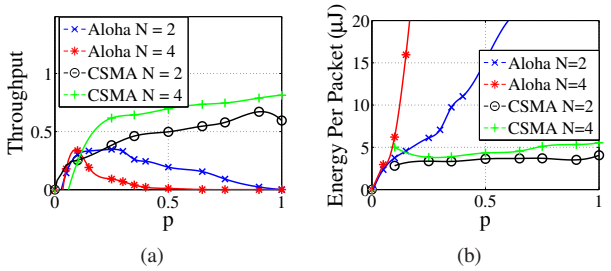

Fig. 12. (a) Average throughput as a function of p, the transmit probability for Aloha and CSMA (100% throughput is 18.5kbps), and (b) average energy spent per successful packet transmission, as a function of p.

protocols have been theoretically analyzed, this is the first attempt to implement and evaluate these well-studied MAC protocols over a UWB-IR physical layer. Additionally, as CSMA requires listening to the channel, which is a relatively energetically expensive operation in UWB-IR, we conducted experiments to assess the tradeoff between the added energy consumption of CSMA and the increased throughput.

For both MAC protocols, Fig. 12 shows experimentally obtained throughput and energy spending values. The evaluations were conducted in networks of 2 and 4 'infinitely backlogged' (i.e., sending as often as possible) EnHANT prototypes. Energy spending per successful packet, shown in Fig. 12(b), was calculated based on transceiver energy consumption data provided in [3] (0.31mW transmitting, 3.9mW idle listening). Clearly, the Aloha throughput curves, shown in Fig. 12(a), bear strong resemblance to classical analytical Aloha results.

Expectedly, CSMA throughput is higher than Aloha's and increases as p increases. Yet, CSMA throughput is lower than the theoretical values, due to a delay between sensing an idle channel and sending a packet, and due to delays imposed by the prototype microcontroller (whose resources are occupied by other processes, i.e., energy monitoring). Additionally, despite the added cost of CCA, the collision avoidance provided by CSMA reduces the average energetic cost per successful packet significantly as compared to Aloha.

C. Higher-Layer Algorithms

On top of the UWB-IR physical layer and CSMA MAC layer, we implemented packet forwarding and routing functionalities in the network layer. To our knowledge, the EnHANTs testbed network is *the first UWB-IR-based multihop network*. Moreover, since communicating energy harvesting nodes need to jointly adapt their higher layer behavior to energy availability, we implemented simple *energy-harvesting-adaptive* link data rate adaptation, flow control, and collection tree adaptation policies (see [6] for more details). The testbed allows extensive evaluation of these policies.

VI. Future Work

Future work will focus on hardware, software, and algorithms that will support the realization of the long-term EnHANTs vision, and on extensive algorithm evaluation using the developed testbed. We will design and integrate hardware components tailored for the future EnHANT form factor, such as thin film batteries and flexible antennas. We will develop MAC protocols for ultra low power UWR-IR communications and lightweight distributed energy harvesting adaptive protocols for large-scale multihop networks of the EnHANTs.

Acknowledgements

We thank students whose projects contributed to the EnHANT prototypes: D. Bendavid, G. Burrow, J. Chen, H. Huang, E. Katz, P. Miller, Z. Noorbhaiwala, D. Piao, D. Roggensinger, A. Schwartz, T. Sharma, D. Shrestha, A. Skolnik, A. Smith, O. Winn, and E. Xu. This work was supported in part by Vodafone Americas Foundation Wireless Innovation Project, United Microelectronics, a grant from Texas Instruments, and NSF grants CNS-0644202, CCF-0964497, CNS-0916263, CNS-0931870, CNS-10-54856. The UWB antennas were provided by Prof. H. Krishnaswamy.

References

[1] "Texas Instruments MSP430 Solar Energy Harvesting Development Tool," focus.ti.com/docs/toolsw/folders/print/ez430-rf2500-seh.html.

[2] S. Chen, P. Sinha, N. Shroff, and C. Joo, "Finite-horizon energy allocation and routing scheme in rechargeable sensor networks," in *Proc. IEEE INFOCOM'11*, Apr. 2011.

[3] M. Crepaldi, C. Li, J. Fernandes, and P. Kinget, "An ultra-wideband impulse-radio transceiver chipset using synchronized-OOK modulation," *IEEE J. Solid-State Circuits*, vol. 46, no. 10, pp. 2284–2299, Oct. 2011.

[4] K.-W. Fan, Z. Zheng, and P. Sinha, "Steady and fair rate allocation for rechargeable sensors in perpetual sensor networks," in *Proc. ACM SenSys'08*, Nov. 2008.

[5] M. Gorlatova, P. Kinget, I. Kymissis, D. Rubenstein, X. Wang, and G. Zussman, "Energy-harvesting active networked tags (EnHANTs) for ubiquitous object networking," *IEEE Wireless Commun.*, vol. 17, no. 6, pp. 18–25, Dec. 2010.

[6] M. Gorlatova, R. Margolies, J. Sarik, G. Stanje, J. Zhu, B. Vigraham, M. Szczodrak, L. Carloni, P. Kinget, I. Kymissis, and G. Zussman, "Prototyping energy harvesting active networked tags (EnHANTs)," Columbia University, Tech. Rep. 2012-07-27, July 2012, available at http://enhants.ee.columbia.edu/images/papers/CU-EE-2012-07-27.pdf.

[7] M. Gorlatova, A. Wallwater, and G. Zussman, "Networking low-power energy harvesting devices: Measurements and algorithms," *To appear in IEEE Trans. Mobile Comput.*, 2013.

[8] R.-S. Liu, P. Sinha, and C. E. Koksal, "Joint energy management and resource allocation in rechargeable sensor networks," in *Proc. IEEE INFOCOM'10*, Mar. 2010.

[9] P. Peumans, A. Yakimov, and S. Forrest, "Small molecular weight organic thin-film photodetectors and solar cells," *J. Appl. Phys.*, vol. 93, 2003.

[10] S. Solda, M. Caruso, A. Bevilacqua, A. Gerosa, D. Vogrig, and A. Neviani, "A 5 Mb/s UWB-IR transceiver front-end for wireless sensor networks in 0.13 CMOS," *IEEE J. Solid-State Circuits*, vol. 46, no. 7, pp. 1636–1647, July 2011.

[11] G. Stanje, P. Miller, J. Zhu, A. Smith, O. Winn, R. Margolies, M. Gorlatova, J. Sarik, M. Szczodrak, B. Vigraham, L. Carloni, P. Kinget, I. Kymissis, and G. Zussman, "Demo: Organic solar cell-equipped energy harvesting active networked tag (EnHANT) prototypes," in *Proc. ACM SenSys'11*, Nov. 2011.

[12] J. Taneja, J. Jeong, and D. Culler, "Design, modeling, and capacity planning for micro-solar power sensor networks," in *Proc. IEEE IPSN'08*, Apr. 2008.

[13] "Powercast development kits," http://www.powercastco.com/products/development-kits/.

[14] Y. Yang, L. Wang, D. K. Noh, H. K. Le, and T. F. Abdelzaher, "SolarStore: Enhancing data reliability in solar-powered storage-centric sensor networks," in *Proc. ACM MobiSys'09*, June 2009.

[15] J. Zhang, P. Orlik, Z. Sahinoglu, A. Molisch, and P. Kinney, "UWB systems for wireless sensor networks," *Proc. IEEE*, vol. 97, no. 2, pp. 313–331, Feb. 2009.